

See discussions, stats, and author profiles for this publication at: <https://www.researchgate.net/publication/266682007>

Reversible Ion Transportation Switch by a Ligand-Gated Synthetic Supramolecular Ion Channel

ARTICLE in JOURNAL OF THE AMERICAN CHEMICAL SOCIETY · OCTOBER 2014

Impact Factor: 12.11 · DOI: 10.1021/ja5070312 · Source: PubMed

CITATIONS

3

READS

46

8 AUTHORS, INCLUDING:



Takahiro Muraoka

Tohoku University

29 PUBLICATIONS 1,108 CITATIONS

[SEE PROFILE](#)



Satoru Nagatoishi

The University of Tokyo

31 PUBLICATIONS 400 CITATIONS

[SEE PROFILE](#)



Kouhei Tsumoto

The University of Tokyo

295 PUBLICATIONS 5,959 CITATIONS

[SEE PROFILE](#)



Kazushi Kinbara

Tokyo Institute of Technology

114 PUBLICATIONS 3,386 CITATIONS

[SEE PROFILE](#)

Reversible Ion Transportation Switch by a Ligand-Gated Synthetic Supramolecular Ion Channel

Takahiro Muraoka,^{*,†,‡} Takahiro Endo,[†] Kazuhito V. Tabata,[§] Hiroyuki Noji,[§] Satoru Nagatoishi,[⊥] Kouhei Tsumoto,^{⊥,||,#} Rui Li,[†] and Kazushi Kinbara^{*,†}

[†]Institute of Multidisciplinary Research for Advanced Materials, Tohoku University, 2-1-1, Katahira, Aoba-ku, Sendai 980-8577, Japan

[‡]PRESTO, Japan Science and Technology Agency, 4-1-8, Honcho, Kawaguchi, Saitama 332-0012, Japan

[§]Department of Applied Chemistry, School of Engineering, The University of Tokyo, Bunkyo-ku, Tokyo 113-8656, Japan

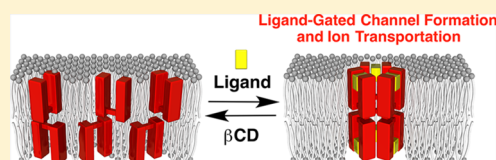
[⊥]Department of Bioengineering, The University of Tokyo, Bunkyo-ku, Tokyo 108-8656, Japan

^{||}Department of Chemistry and Biotechnology, The University of Tokyo, Bunkyo-ku, Tokyo 108-8656, Japan

[#]Institute of Medical Science, The University of Tokyo, 4-6-1, Shirokanedai, Minato-ku, Tokyo 108-8639, Japan

S Supporting Information

ABSTRACT: Inspired by the regulation of cellular activities found in the ion channel proteins, here we developed membrane-embedded synthetic chiral receptors **1** and **2** with different terminal structures, where receptor **1** has hydrophobic triisopropylsilyl (TIPS) groups and receptor **2** has hydrophilic hydroxy groups. The receptors have ligand-binding units that interact with cationic amphiphiles such as 2-phenethylamine (PA). Conductance study revealed that the receptors hardly show ion transportation at the ligand-free state. After ligand binding involving a conformational change, receptor **1** bearing TIPS termini displays a significant current enhancement due to ion transportation. The current substantially diminishes upon addition of β -cyclodextrin (β CD) that scavenges the ligand from the receptor. Importantly, the receptor again turns into the conductive state by the second addition of PA, and the activation/deactivation of the ion transportation can be repeated. In contrast, receptor **2** bearing the hydroxy terminal groups hardly exhibits ion transportation, suggesting the importance of terminal TIPS groups of **1** that likely anchor the receptor in the membrane.



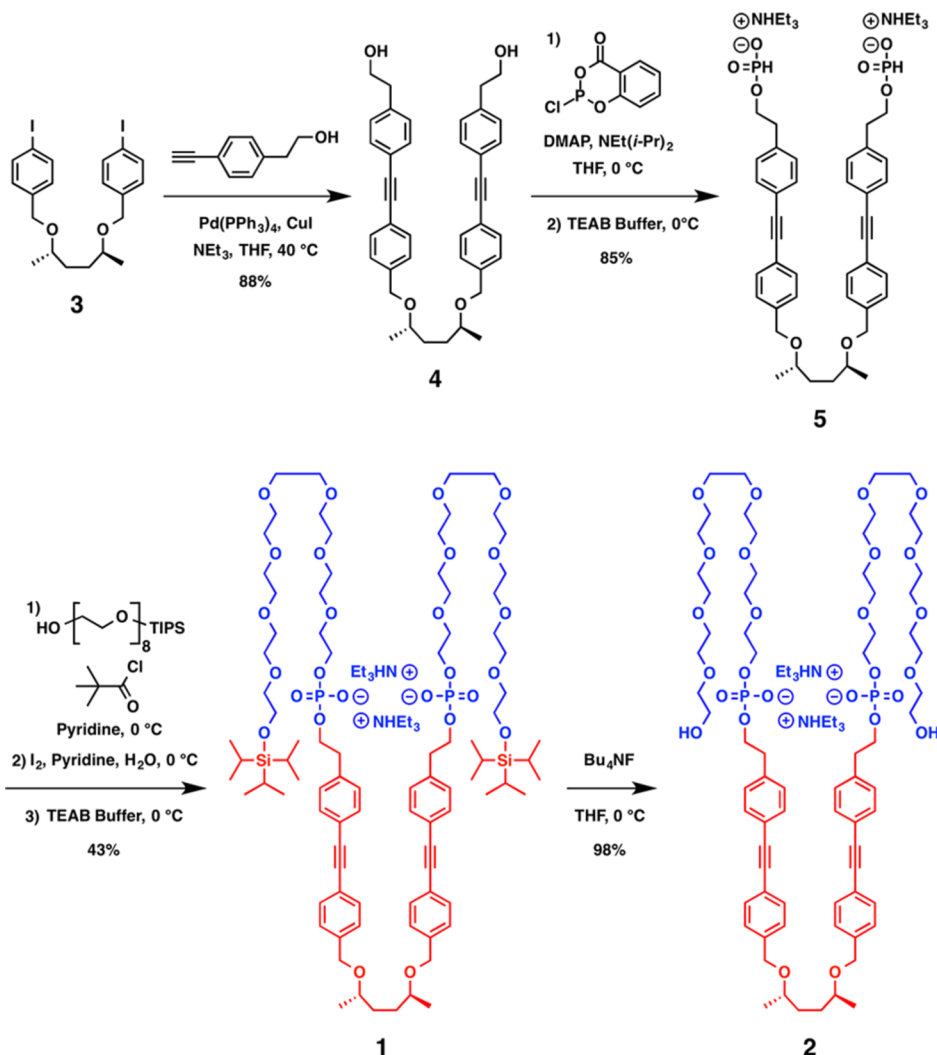
INTRODUCTION

Signal transduction through a cytoplasmic membrane is an important function for regulation of vital activities,¹ where the membrane proteins play essential roles. One of the typical mechanisms included in the signal transduction is a reversible switch of ion transportation in response to input signals, such as a ligand,² light,³ and mechanical force.⁴ For example, cyclic nucleotide-gated ion channels recognizes cyclic nucleotides as ligands, which triggers opening of the channel for the cation transportation.^{2a,b} Such sophisticated mechanisms realized by the membrane proteins provides various hints for design of dynamic synthetic organic devices. In fact, synthetic and semisynthetic ion channels capable of responding to physical stimuli such as light has been developed so far,⁵ for possible applications to regulation of cellular activities, photopharmacology, and optogenetics. In contrast, in spite of being widespread in nature, reversibly operative ligand-gated ion channels remain mostly unexplored by synthetic molecules.⁶ In this context, Matile and co-workers have reported pioneering examples of synthetic ion channels operative by a ligand-gating mechanism, where a topological change of the supramolecular architecture from the twisted to the barrel-stave forms is triggered by intercalation of electron-rich aromatic ligands to open the channel.⁷ In these systems, additional reagents, which plug the lumen of the channel, are able to shut the channel irreversibly. Likewise, most subsequently reported ligand-responsive

synthetic channels operate irreversibly, and undergo opening or closing (blocking)⁸ gates by addition of ligands. To the best of our knowledge, the only successful example of a synthetic ion channel with reversible gating function was reported by a metal coordination system, where an inorganic additive, palladium(II), allows the channel formation by the coordination with the bidentate ligand embedded in the membrane, while subsequent addition of a palladium(II)-chelating agent dissociates the complex to deactivate the ion transportation.⁹

In our previous studies on the multiblock amphiphilic foldamers composed of repeating hydrophilic and aromatic hydrophobic moieties,¹⁰ we have developed a tetrameric molecule adopting a folded geometry in the membranes, which assembles into a tetrameric supramolecular structure acting as an ion channel. In the course of subsequent studies on the stimuli responsive amphiphilic molecules, we have developed **1** (Scheme 1), having an alternately aligned hydrophobic and hydrophilic sequences consisting of a chiral hydrophobic core bearing two diphenylacetylene (DPA) units, and hydrophilic octaethylene glycol (OEG) chains connected via phosphoric ester linkage. We found that **1** is able to be embedded into a bilayer with a folded bent conformation, where the two DPA and phosphoric ester units come close to

Received: July 11, 2014

Scheme 1. Synthetic Route of Receptors 1 and 2^a

^aThe red and blue parts in **1** and **2** denote the hydrophobic and hydrophilic units, respectively.

each other at the interface between the membrane and aqueous media allowing them to bind with an aromatic amine. Interestingly, **1** shows reversible gating of ion transportation in response to the addition and removal of the ligand. In the present article, we report the details of the properties of **1** including its reversible ligand-responsive ion transport across a lipid membrane.

RESULTS AND DISCUSSION

Synthesis of Receptors 1 and 2. Synthesis of **1** and **2** was started from the construction of the hydrophobic part followed by the conjugation of the hydrophilic OEG chains via phosphoric ester linkage (Scheme 1). Williamson ether synthesis between (2S,5S)-hexane-2,5-diol and 1-(bromomethyl)-4-iodobenzene using NaH in tetrahydrofuran (THF) gave **3** in 92% yield. **3** was coupled with 2-(4-ethynylphenyl)ethanol¹¹ catalyzed by Pd(PPh₃)₄ and CuI in NEt₃ and THF to afford **4** in 88% yield. Then, **4** was converted into *H*-phosphonate monoester **5** by phosphitylation with van Boom's reagent¹² and a catalytic amount of *N,N*-dimethyl-4-aminopyridine (DMAP) in NEt(i-Pr)₂ and THF, followed by a treatment with 1.0 M triethylammonium bicarbonate (TEAB, pH 8.5) buffer. Finally, **5** was condensed with OEG bearing a triisopropylsilyl (TIPS)

group in the presence of pivaloyl chloride in pyridine, followed by the treatment with TEAB (pH 8.5) to afford **1** as colorless oil in 43% yield. In addition, deprotection of the TIPS groups of **1** with tetra-*n*-butylammonium fluoride provided **2** as colorless oil in 98% yield. The synthetic products were unambiguously characterized by ¹H, ¹³C and ³¹P nuclear magnetic resonance (NMR) spectroscopy and matrix assisted laser desorption/ionization time-of-flight (MALDI-TOF) mass and electrospray ionization time-of-flight (ESI-TOF) mass spectrometry.

Conformational Study of Receptors 1 and 2 in THF and Water. Before investigating the properties of **1** and **2** in the lipid membranes, we have carried out NMR and circular dichroism (CD) spectroscopic studies of **1** and **2**, focusing on their conformations in solvents with different polarity. As expected, the bolaamphiphiles **1** and **2** formed aggregates in aqueous environment while they are soluble in organic solvents like THF and CHCl₃.

¹H NMR spectrum of **1** in THF-*d*₈ (5.0 mM) at 20 °C showed sharp signals corresponding to the protons of DPA rings at 7.33, 7.34, 7.47, and 7.50 ppm (Figure 1a). Addition of D₂O (25% v/v) to the THF-*d*₈ solution of **1** induced upfield shift of these signals (7.25, 7.28, 7.33, and 7.36 ppm, Figure

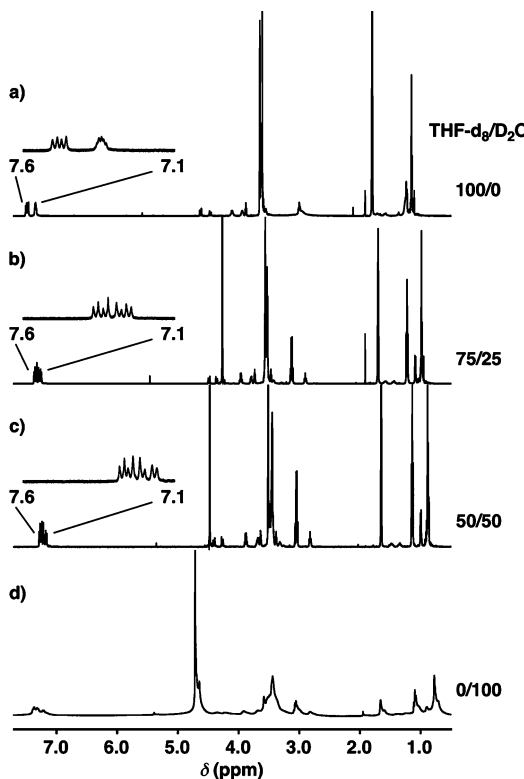


Figure 1. ^1H NMR spectra of **1** (5.0 mM) in the mixtures of THF- d_8 /D₂O = (a) 100/0, (b) 75/25, (c) 50/50, and (d) 0/100 (v/v) at 20 °C.

1b), and this trend was kept by further addition of D₂O up to 50% (7.17, 7.21, 7.25, and 7.27 ppm, 5.0 mM, Figure 1c). These spectral changes induced by the solvent polarity increment are likely due to the enhanced magnetic shielding by aromatic groups, suggesting that DPA units assemble together by intramolecular or intermolecular interactions. The hydrodynamic radii of **1** at 20 °C in THF- d_8 (D_h _{THF}) and in 1:1 mixture of THF- d_8 and D₂O (D_h _{THF-Water}), evaluated by diffusion-ordered NMR spectroscopy (DOSY), are almost comparable with each other (D_h _{THF} = 1.35 nm, D_h _{THF-Water} = 1.41 nm).¹³ These values are consistent with the molecular size of **1** calculated by a molecular modeling (1.40 nm),¹⁴ indicating that **1** hardly aggregates under these conditions. Hence, these NMR experiments represent that, while **1** adopts a rather extended conformation in THF, addition of water induces a bent conformation presumably due to hydration and also the hydrophobic and aromatic interactions, where the two DPA units are in close proximity, as schematically illustrated in Scheme 2.

Thanks to the chirality of **1**, the conformational change around the DPA units could be visualized by CD spectroscopy. As shown in Figure 2a (red line), **1** in THF (3.4 μM, 20 °C) showed weak Cotton effect at wavelengths corresponding to the absorption of the DPA units (260–320 nm). In a 90/10 mixture of THF/water (v/v), positive (285–320 nm) and relatively weak negative (260–285 nm) CD signals appeared, and they were further intensified in the 50/50, 25/75 and 0/100 mixtures. The CD spectra of **1** in water hardly showed concentration dependence in the range of $[1] = 0.034$ –3.4 μM, below its critical aggregation concentration¹⁵ (see Supporting Information, Figure S2a), suggesting that the CD signals are mostly originated from the chiral geometry of the molecule

Scheme 2. Schematic Drawing of the Folding of **1 in Response to the Solvent Polarity Increment**

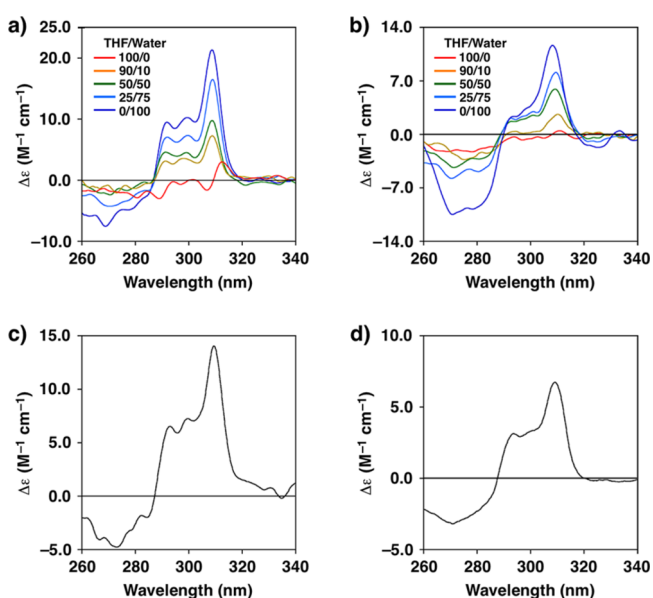
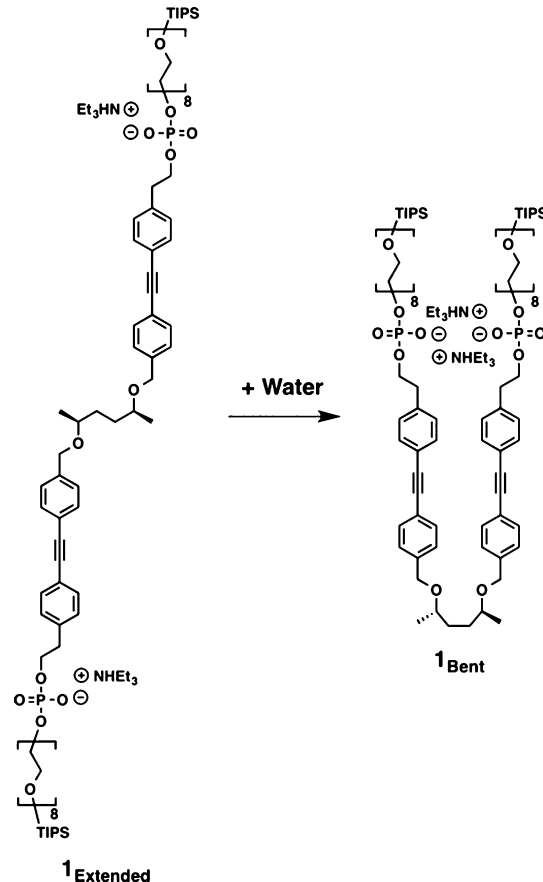


Figure 2. CD spectra of (a) **1** and (b) **2** in THF/water mixtures (3.4 μM, THF/water = 0/100, 25/75, 50/50, 90/10, and 100/0 v/v) at 20 °C and those of DOPC-LUVs ([DOPC] = 0.18 mM) containing (c) **1** and (d) **2** ($[1] = [2] = 0.020$ mM) in water at 20 °C. The absorption spectra corresponding to (a, b) and (c, d) are shown in the Supporting Information, Figure S1 and Figure S9, respectively.

itself. Considering that the rigid chiral molecules bearing chromophores in close proximity tend to show strong CD

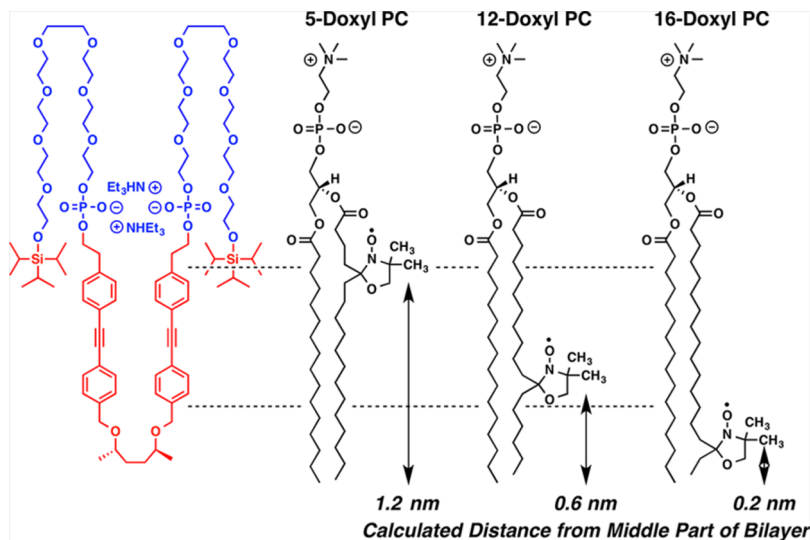


Figure 3. Structural formulas of **1**, 5-Doxyl, 12-Doxyl, and 16-Doxyl PCs to schematically show the positional relationships between the DPA units and the doxyl groups.

signals,^{16,17} **1** likely adopts a relatively flexible conformation in THF, which changes into a more rigid geometry by addition of water to form the bent conformation (Scheme 2). It should be noted here that in D_2O , **1** (5.0 mM) showed broadened 1H NMR signals, suggesting self-assembly (Figure 1d). Indeed, dynamic light scattering (DLS) measurement visualized 200 nm size aggregates (see Supporting Information, Figure S5).

In analogy with **1**, **2** showed enhancement of the negative (260–290 nm) and positive (290–320 nm) CD-signal intensities upon addition of water to THF (Figure 2b, red to blue lines). The CD spectral profile of **2** in water was similar to **1**, also suggesting that **2** adopts a bent conformation with the two DPA units stacked in water, while adopting an extended flexible conformation in THF. It is noteworthy again here that concentration dependency was hardly observed in the CD spectra of **2** in water in the concentration range of 0.034–3.4 μM (see Supporting Information, Figure S2b), indicating that the CD signals also originate from the conformation of the molecule, and not from the self-assembly.

Conformation of Receptors **1 and **2** in Bilayer Membrane.** **1** and **2** were introduced in a phospholipid bilayer of giant unilamellar vesicles (GUVs), which can be directly observed by optical microscopy. GUVs composed of 1,2-dioleoyl-*sn*-glycero-3-phosphocholine (DOPC) and **1** or **2** ($[DOPC] = 0.18 \text{ mM}$, $[1] = [2] = 0.020 \text{ mM}$) were prepared by the gentle hydration method,¹⁸ where phase-contrast microscopy displayed the successful formation of GUVs in water (see Supporting Information, Figure S6). These GUVs could also be visualized under a fluorescence microscope monitoring >420 nm-light with excitation of the DPA units of **1** and **2** ($\lambda_{ex} = 330\text{--}385 \text{ nm}$), which demonstrates successful incorporation of **1** and **2** into the phospholipid bilayer. Since the fluorescence was observed uniformly over the whole membrane, **1** and **2** are likely dispersed in the bilayer without lateral phase separation such as a raft formation.

The location and orientation of **1** and **2** in the bilayer were studied by a fluorescence depth quenching method.¹⁹ Since the efficiency of fluorescence quenching depends on the distance between a spin probe and a fluorescent chromophore, this method allows for the investigation of the geometry of the DPA units in the lipid bilayer. Three spin-labeled phospholipids, **1**

palmitoyl-2-stearoyl-(5-doxy)-*sn*-glycero-3-phosphocholine (5-Doxy PC), 1-palmitoyl-2-stearoyl-(12-doxy)-*sn*-glycero-3-phosphocholine (12-Doxy PC), and 1-palmitoyl-2-stearoyl-(16-doxy)-*sn*-glycero-3-phosphocholine (16-Doxy PC), bearing a spin probe at different positions in the alkyl tails were used for the present study (Figure 3). The molecular modeling (Molecular Mechanics with an MMFF force field using Spartan'10) showed that the spin probes of 5-, 12-, and 16-Doxy PCs locate at 1.2, 0.6, and 0.2 nm away from the center of the DOPC bilayer, respectively. DOPC large unilamellar vesicles including **1** or **2** (DOPC·**1**-LUVs, DOPC·**2**-LUVs) with/without a Doxyl PC were prepared by freezing-and-thawing followed by sonication. DLS analyses exhibited the formation of LUVs with 275 and 154 nm mean diameter for DOPC·**1**-LUV and DOPC·**2**-LUV, respectively ($[\text{total phosphocholines}] = 0.18 \text{ mM}$, $[1] = [2] = 0.020 \text{ mM}$, see Supporting Information, Figure S7). Incorporation of 10 mol % 16-Doxy PC into DOPC·**1**-LUVs resulted in 46% decrease of the fluorescence intensity of **1** at 340.0 nm (see Supporting Information, Figure S8a). On the other hand, 10 mol % of 5- and 12-Doxy PCs comparably quenched the fluorescence of **1** at 340.0 nm with higher efficiency than 16-Doxy PC (58 and 56% decrease, respectively). Likewise, for DOPC·**2**-LUVs, 5-Doxy and 12-Doxy PCs comparably showed higher quenching efficiency for the fluorescence at 369.0 nm (56 and 54% decrease, respectively; see Supporting Information, Figure S8c) than 16-Doxy PC (43%). Thus, the DPA units of **1** and **2** likely locate inside the lipid bilayer at the depth between 5- and 12-position of the dodecyl group, and mostly in parallel with the alkyl chains of DOPC (Figure 3).

CD spectra of DOPC·**1**-LUVs suspension in water ($[DOPC] = 0.18 \text{ mM}$, $[1] = 0.020 \text{ mM}$, Figure 2c) exhibited fairly similar spectrum to that of **1** in water (Figure 2a, blue line). DOPC·**2**-LUVs also showed an analogous CD pattern ($[DOPC] = 0.18 \text{ mM}$, $[2] = 0.020 \text{ mM}$, Figure 2d) to **2** alone in water (Figure 2b, blue line). Hence, it is suggested that **1** and **2** embedded in the DOPC bilayer adopt a bent conformation with an intramolecular stacking of the DPA units. It is known that self-assembly of aromatic units is encouraged in a nonpolar paraffinic solvent by $\pi\text{--}\pi$ interaction.^{20,21} Since the lipid segment in the bilayer is filled with alkyl chains, the $\pi\text{--}\pi$

stacking between the DPA units of the receptors is likely favorable. Thus, it is considered that the bent conformations of **1** and **2** are stabilized by the $\pi-\pi$ stacking as well as hydration at the phosphoric ester groups and the OEG chains.

Considering the length of the hydrophobic parts of **1_{Bent}** and **2_{Bent}** (1.54 nm), **1** and **2** adopting bent conformations are likely fit in the DOPC monolayer in the bilayer membrane (see Supporting Information, Figure S10a). This is supported by the fluorescence depth quenching experiments described above, which suggests that the DPA units are located between the 5- and 12 positions of DOPC alkyl chain. To further investigate the detailed conformations of **1** and **2** in the bilayer, especially focusing on the location of the terminal groups of **1** (TIPS groups) and **2** (OH groups), the areas per molecule (A) of **1** and **2** were evaluated in the Langmuir–Blodgett (LB) monolayer of DOPC. The surface pressure was measured in both monolayers ($[1]/[\text{DOPC}] = [2]/[\text{DOPC}] = 1/9$) from the gas and liquid-expanded (G-LE) phase to the collapsed state, via the liquid-expanded (LE) and liquid-condensed (LC) phases (Figure 4). The linear extrapolation of the LC phase

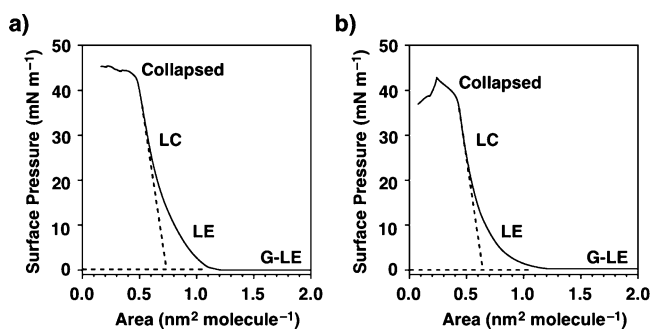


Figure 4. Isotherms of Langmuir–Blodgett monolayers composed of the mixture of DOPC and (a) **1** or (b) **2** ($[1]/[\text{DOPC}] = [2]/[\text{DOPC}] = 1/9$) compressed at $23.3 \text{ mm}^2 \text{ s}^{-1}$ at 20°C . G-LE, LE, and LC denote the coexistence of gas and liquid-expanded phases, liquid-expanded phase, and liquid-condensed phase, respectively. The broken lines are guides for linear extrapolation of the LC phase transition line to the surface pressure $\pi = 0$.

transition lines to surface pressure $\pi = 0 \text{ mN m}^{-1}$ gives the average areas of mixtures of DOPC (90-mol %) with **1** and **2** (10-mol %) at $\pi = 0 \text{ mN m}^{-1}$ to be 0.72 and 0.67 nm^2 , respectively.²² On the basis of these values and the reported A value of DOPC (0.691 nm^2),²³ A values of **1** and **2** in DOPC monolayer were evaluated to be $A_{1(\text{DOPC})} = 1.0 \text{ nm}^2$ and $A_{2(\text{DOPC})} = 0.43 \text{ nm}^2$, respectively. Here, $A_{2(\text{DOPC})}$ are close to the calculated sectional area of the hydrophobic unit ($S_{\text{Hydrophobic}} = 0.441 \text{ nm}^2$, see Supporting Information, Figure S10b), suggesting that **2** adopts a bent conformation in the DOPC monolayer with the terminal OH groups in the aqueous phase as shown in Figure 5b. Importantly, the larger value of A_1 than A_2 suggests that the two TIPS groups of **1** are embedded inside the membrane. Indeed, the sum of the calculated sectional areas of $2S_{\text{DPA}}$ and two TIPS groups is 1.11 nm^2 , which is close to $A_{1(\text{DOPC})}$. Thus, it is strongly likely that **1** and **2** in the DOPC monolayer adopt “M-shape” and “V-shape” conformations, respectively (Figure 5).

Guest-Binding Capability of Receptors **1 and **2** in Bilayer Membrane.** β -Adrenergic receptor is a membrane protein belonging to a class of G protein-coupled receptors, which recognizes aromatic amines. It has been proposed that the receptor interacts with the guest mainly through the

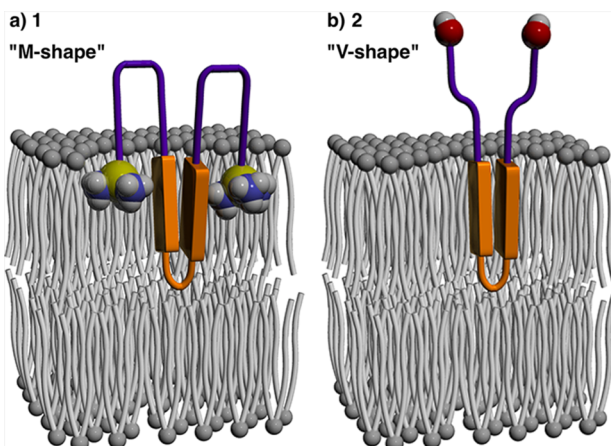


Figure 5. Schematic drawing of the conformations of (a) **1** and (b) **2** adopting “M-shape” and “V-shape” conformations in a DOPC bilayer (gray), respectively. The terminal TIPS and hydroxy groups of **1** and **2** are represented in space-filling models, where yellow, light blue, red, and white spheres denote silicon, carbon, oxygen, and hydrogen atoms, respectively. Orange plates denote the DPA units, which are connected with the 2,5-bisoxohexane linker represented as an orange tube.

electrostatic interaction between the anionic carboxylate groups at the guest recognition site and the cationic ammonium group of the guest with an assistance of $\pi-\pi$ interaction between the aromatic groups.²⁴ This mechanism gave us an idea that the anionic phosphodiester groups and aromatic DPA units of **1** and **2** could provide an interaction site for amines bearing aromatic groups, such as phenethylamine (PA).²⁵

Upon addition of PA into DOPC-**1**-LUVs suspension in water ($[\text{DOPC}] = 0.18 \text{ mM}$, $[\mathbf{1}] = 0.020 \text{ mM}$, 20°C), CD spectra showed a negative-to-positive signal transition at 260 – 285 nm , together with slight decrease of the positive CD signal at 290 – 315 nm (Figure 6a). The sharp positive Cotton effect observed at 309 nm shifted to 311 nm with an isodichroic point at 312 nm , where the CD spectral change reached a plateau at $[\text{PA}]/[\mathbf{1}] > 1000$. In the absorption spectroscopy (see, Supporting Information, Figure S9a), the absorption bands corresponding to the DPA unit (287 and 305 nm) displayed red-shift (289 and 307 nm , respectively). Similarly, the intensities of the negative (260 – 285 nm) and positive (290 – 315 nm) CD signals of DOPC-**2**-LUVs suspension in water ($[\text{DOPC}] = 0.18 \text{ mM}$, $[\mathbf{2}] = 0.020 \text{ mM}$, 20°C) decreased with an isodichroic point at 315 nm by addition of PA, together with red-shift of the CD signal from 309 to 311 nm , where the spectral change leveled off at $[\text{PA}]/[\mathbf{2}] > 1000$ (Figure 6b). Absorption bands corresponding to the DPA units of **2** showed red-shift during this CD spectral change (288 – 290 nm and 307 – 309 nm , see Supporting Information, Figure S9b), in analogous to **1**. Thus, both **1** and **2** likely interact with PA in the DOPC bilayer, accompanied by the conformational changes around the DPA unit. It should be noted here that the CD signal intensity of **2**-PA in the bilayer was considerably smaller than that of **1**-PA (Figure 6a,b, blue lines), suggesting a smaller twisting angle between the two DPA units in **2**-PA than in **1**-PA.^{16,26}

It is noteworthy here that, the fluorescence spectrum of DOPC-**1**-LUVs displayed the peak at 340 nm (see Supporting Information, Figure S12a, red line), and upon titration of PA up to $[\text{PA}]/[\mathbf{1}] = 100$, a monotonic slight decrease of the fluorescence intensity was observed with almost unchanged

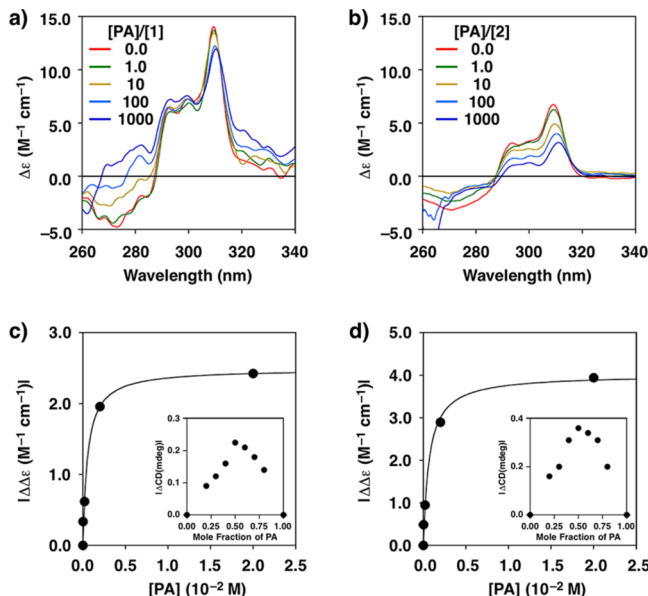


Figure 6. CD spectral changes of DOPC-LUVs ($[DOPC] = 0.18$ mM) containing (a) **1** and (b) **2** ($[1] = [2] = 0.020$ mM) in water at $20^\circ C$ upon titration with phenethylamine (PA) at $[PA]/[1] = [PA]/[2] = 0.0, 1.0, 10, 100$, and 1000 . The corresponding absorption spectra are shown in Supporting Information, Figure S9. Curve fitting analyses of the CD signal changes of (c) DOPC·1-LUV and (d) DOPC·2-LUV ($[DOPC] = 0.18$ mM, $[1] = [2] = 0.020$ mM, 309.4 and 309.2 nm, respectively) as a function of PA concentration ($[PA] = 0.0, 0.020, 0.20, 2.0$, and 20 mM), where the absolute values of the CD signal changes were plotted. Inset: Job plots for stoichiometry determination of the complexation of membrane-embedded (c) **1** and (d) **2** with PA on the basis of the CD signal intensities (309.4 and 309.2 nm, respectively).

spectral profile. At $[PA]/[1] = 300$, the fluorescence intensity around 370 nm increased (see Supporting Information, Figure S12a, yellow line), and the highest peak shifted to 373 nm at $[PA]/[1] > 500$. Here, the spectral changes of CD and fluorescence spectra did not occur synchronously with respect to the concentration of PA (see Supporting Information, Figure S12b). As described above, the CD study of **1** in the solution of THF and water indicated that CD signals of **1** are mostly originated from the chiral geometry of the molecule itself. Meanwhile, it is reported that self-assembled DPA shows fluorescence around 380 nm.²⁷ Hence, it is likely that the CD and fluorescence spectral changes are due to a conformational change followed by intermolecular assembly of **1** encouraged by addition of PA.

The dissociation constants K_d between PA and the receptors embedded in the DOPC bilayer were evaluated by curve fitting analyses of the CD signal changes and Biacore surface plasmon resonance (SPR) assay. The CD signal intensity (in absolute value format) of DOPC·1 (309.4 nm) and DOPC·2 (309.2 nm) as a function of PA concentration are shown in Figure 6c,d, together with Job plots shown as insets. For precise evaluation of the receptors' concentrations engaging in the complexation with PA, DOPC·1-LUV and DOPC·2-LUV for these plots were prepared by hydration of a mixture of DOPC and **1** or **2** in aqueous solutions of PA ($[PA] = 0.0, 0.020, 0.20, 2.0$, and 20 mM). This procedure allows PA to be incorporated in both outer and inner layers of the LUVs and interact with **1** and **2**. Job plots of **1** and **2** with PA showed the maxima at the molar fractions of 0.5, suggesting 1:1 complexation between the

receptors and PA at the bilayer. Curve fitting analyses of the plots in Figure 6c,d gave the dissociation constants $K_d(1\text{-PA}) = 443 \mu M$ and $K_d(2\text{-PA}) = 577 \mu M$, respectively, for the 1:1 complexation. The dissociation constant between **1** and PA was further investigated by SPR (Figure 7a) using the Biacore

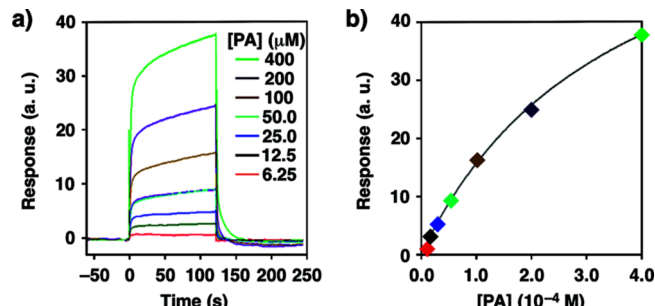


Figure 7. (a) A Biacore surface plasmon resonance (SPR) sensogram displaying the binding response between **1** and PA in the function of time, where the subtracted SPR responses between the sample and reference cells were plotted. Bilayers composed of a mixture of DOPC and **1** ($[1]/[DOPC] = 1/9$) and DOPC alone were immobilized onto Biacore Sensor Chip L1 for the sample and reference cells, respectively, which was treated with PA in HEPES buffer ($[PA] = 6.25, 12.5, 25.0, 50.0, 100, 200$, and $400 \mu M$, 20 mM HEPES, 50 mM KCl, 2.0 mM MgCl₂, pH 7.5) at $20^\circ C$. (b) A plot of the SPR responses in the function of the concentration of PA.

system. By the curve fitting analysis of the plot between the SPR response and the PA concentration, K_d between **1** and PA at the bilayer was evaluated to be $K_d(1\text{-PA}) = 370 \mu M$ (Figure 7b), which is in good agreement with the K_d value evaluated on the basis of the CD measurement.

Ion Transportation Activities of Receptors **1 and **2** in Bilayer Membrane in Response to Guest-Docking.** A mixture of DOPC and **1** or **2** ($[DOPC] = 12.7$ mM, $[1] = [2] = 10$ nM) in *n*-decane was painted on an orifice with a diameter of $150 \mu m$, which provides a planar DOPC bilayer containing **1** or **2** uniformly in the both sides. The orifice was sandwiched by two chambers (upper *cis* and lower *trans* chambers) containing HEPES buffer (20 mM HEPES, 50 mM KCl, 2.0 mM MgCl₂, pH 7.5, 0.30 mL each). The currents were recorded as a function of time at $20^\circ C$. DOPC bilayer containing **1** hardly showed current at the applied voltage of +80 mV (Figure 8a), and addition of PA ($0.20 \mu M$) into the upper chamber hardly affects the current profile (Figure 8b, **1** + PA^U). However, interestingly, subsequent addition of PA ($0.20 \mu M$) into the lower chamber triggered a significant increase in the current flow.²⁸ In the conductance profile, pulsed currents with average flows of 4.9 pA and 10.8 pA were observed, likely corresponding to singly and doubly formed ion channels, respectively (Figure 8c, **1** + PA^{U&L}).²⁹ The average frequency of the single channel was $22 s^{-1}$. The relationship between the inner diameter d and the conductance g of an ion channel (61 pS) is known to be described by the Hille equation,³⁰

$$\frac{1}{g} = \frac{l\rho}{\pi(d/2)^2} + \frac{\rho}{2}$$

where l and ρ are the length of the channel (3.5 nm) and resistivity of the recording solution ($2.35 \Omega m$), respectively. By solving the equation including the Sansom correction factor,³¹ d was estimated to be 0.87 nm. Considering the size of the

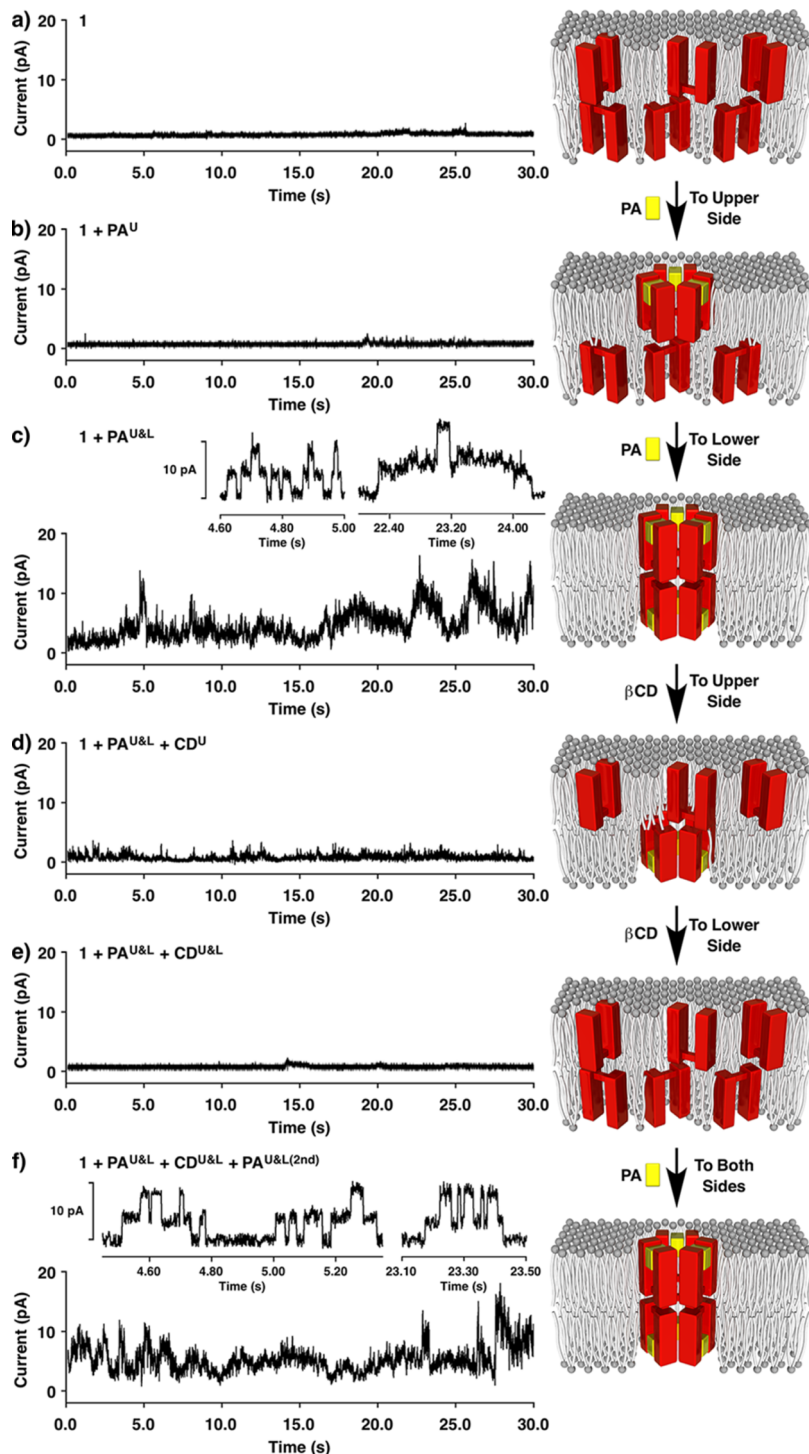


Figure 8. Conductance recordings at the applied voltage of +80 mV of a DOPC bilayer membrane containing **1** (10 nM) in HEPES buffer (20 mM HEPES, 50 mM KCl, 2.0 mM MgCl₂, pH 7.5) (a) before and (b) after the addition of PA (0.20 μM) into the upper chamber (*cis*) (c) followed by the addition into the lower chamber (*trans*) at 20 °C. (d) Subsequently, βCD (5.0 mM) was further added into the upper and (e) lower chambers ([total PA] = 50 nM), (f) followed by the second addition of PA (0.20 μM) into the both chambers. Enlarged views are inserted in (c) and (f) as insets. Schematic drawing of the ligand-response of **1** is shown on the right side. Red, yellow and gray parts denote the hydrophobic unit of **1**, PA, and DOPC, respectively.

single molecule of **1**, this value suggests the formation of supramolecular channel.

It is known that β-cyclodextrin (βCD) interacts with PA in aqueous media with the dissociation constant $K_d = 41.0 \text{ mM}$.³² In fact, by adding βCD (5.0 mM) into the upper chamber to drive the equilibrium of **1** to the unbound state, the frequency

of the current flows significantly reduced to be 2.3 s^{-1} (Figure 8d, **1** + PA^{U&L} + CD^U), and current flow was hardly observed after further addition of βCD (5.0 mM) into the lower chamber (Figure 8e, **1** + PA^{U&L} + CD^{U&L}).³³ It is of importance that the current flow was again enhanced by adding more quantity of PA (0.20 μM) into the both chambers to shift the equilibrium

of **1** to the guest-bound state (Figure 8f, **1** + PA^{U&L} + CD^{U&L} + PA^{U&L(second)}).³⁴ Namely, it is clearly demonstrated that the complexation of **1** with PA significantly enhances the ion transportation activity for potassium, while β CD is able to remove PA from **1** to deactivate the transportation reversibly.

The detachment of PA from **1** by β CD was supported by CD spectroscopic analysis. As written above, **1** in DOPC bilayer shows the maximum positive CD signal at 309 nm (Figures 6a and 9, red lines), which shifts to 311 nm with a decrement of

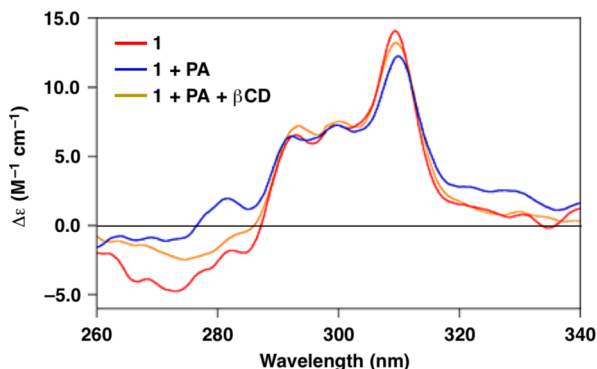


Figure 9. A CD spectral change of DOPC·1-LUVs ($[DOPC] = 0.18$ mM, $[1] = 0.020$ mM) before (red) and after the addition of PA (2.0 mM, blue) followed by the addition of β CD (15 mM, orange).

the intensity upon complexation with PA (Figures 6a and 9, blue lines). Here, addition of β CD to the mixture of **1** and PA resulted in opposite spectral change, where the positive CD signal showed blue-shift with an enhancement of the intensity (Figure 9, orange line), suggesting the backward conformational change of **1** to adopt the uncomplexed geometry.

The ion transportation by **1**·PA was also investigated with vesicles, by monitoring a fluorescence change using a pH sensitive probe. DOPC·1-LUVs encapsulating 8-hydroxypyrene-1,3,6-trisulfonate (HPTS) and PA in the internal aqueous phase (DOPC·1-LUVs \supset HPTS·PA; $[DOPC] = 0.18$ mM, $[1] = 0.010$ mM, $[HPTS] = 30$ μ M, $[PA]_{\text{inside}} = 20$ mM) were prepared in 20 mM HEPES (pH 7.1, containing 50 mM KCl) buffer. HPTS emits 510 nm fluorescence upon excitation with 450 nm light at pH higher than 5, and the fluorescence intensity increases upon enhancement of pH.³⁵ In the absence of PA outside the LUV, DOPC·1-LUVs \supset HPTS·PA showed little increment of the fluorescence intensity (Figure 10a, blue line) after the addition of KOH to increase the pH by 0.8. In contrast, in the presence of PA outside the LUV ($[PA]_{\text{outside}} = 20$ mM), DOPC·1-LUVs \supset HPTS·PA display elevation of the fluorescence intensity (Figure 10a, red line), indicating enhancement of pH due to the transportation of potassium ions. The dependency of the cation transportation rate on the concentration of **1** was nonlinear (Figure 10b), where the curve fitting analysis by Hill equation³⁶ afforded the Hill coefficient $n = 3.1$ ($R^2 = 0.995$). Namely, the number of **1**·PA molecules constructing the ion channel is likely multiple of three. Considering the molecular size of **1**·PA and the pore size (0.87 nm) evaluated by the Hille equation, it is most likely that two half channels of trimeric assembly of **1**·PA complex stack with each other to form the subnm size supramolecular channel (Figure 8, schematic models).

In sharp contrast to **1**, **2** hardly showed ion transportation capability in either presence or absence of PA. A planar DOPC bilayer containing **2** (10 nM) scarcely exhibited conductance at

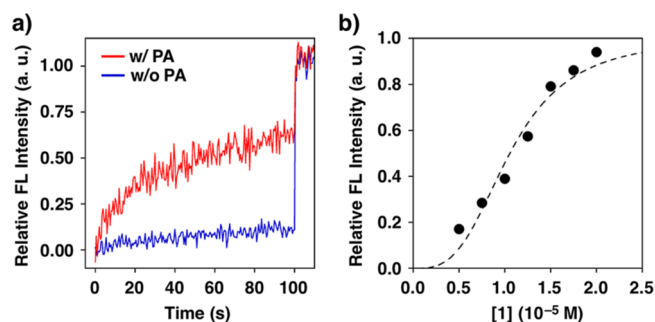


Figure 10. (a) Changes in fluorescence intensity of HPTS (30 μ M) in DOPC·1-LUVs \supset HPTS·PA ($[DOPC] = 0.18$ mM, $[1] = 0.010$ mM, $[PA]_{\text{inside}} = 20$ mM) in 20 mM HEPES buffer containing 50 mM KCl (pH 7.1) at 20 $^{\circ}$ C (excitation at 460 nm, emission at 510 nm) in the presence (red) or absence (blue) of 20 mM PA outside the vesicles as a function of time after the addition of KOH at 0 s followed by the addition of 1.0 wt % triton X-100 at 100 s. $\Delta p\text{H} = 0.8$ (7.1 to 7.9). (b) Concentration dependency of the relative 510 nm fluorescence intensity of HPTS in DOPC·1-LUVs \supset HPTS·PA in the presence of PA outside the vesicles at 30 s after the addition of KOH in 20 mM HEPES buffer containing 50 mM KCl at 20 $^{\circ}$ C. Fitted curve calculated by the Hill equation is drawn as a dashed line.

+80 mV (see Supporting Information, Figure S14a). Although **2** interacts with PA as indicated by the CD spectroscopic study (Figure 4b), the addition of PA into the upper and lower chambers hardly induced the enhancement of the current flows (see Supporting Information, Figure S14b,c). As described above, the conformational studies of **1** and **2** in a DOPC membrane by CD and LB techniques indicated that **1** and **2** adopt “M-shape” and “V-shape” folded conformations, respectively. Namely, the two TIPS groups of **1** are embedded in the hydrophobic alkyl layer of DOPC bilayer, and possibly play roles like anchors in the membrane, which is likely advantageous to the formation of channels.³⁷ Although the complete mechanism of the ion-channel formation of **1**·PA is not fully clarified yet, charge screening and conformational change of **1** induced by the complexation with PA likely fosters the half-channel formation by ionic and van der Waals interactions, thereby allowing formation of the ion channel by assembly of the half-channels with van der Waals interaction. In addition, CD studies suggested that the two DPA units of **1** adopt more twisted geometry than **2**, both before and after the complexation with PA, which is possibly due to the bulkiness of the hydrophobic TIPS groups. Such structural differences between **1** and **2** are considered to result in the contrasting response of the ion transportation induced by the ligand-binding.

CONCLUSIONS

Inspired by the ligand-gated membrane proteins that switch the ion transportation capability reversibly by ligand-triggered conformational changes, we developed membrane-embedded amphiphilic chiral receptors bearing a ligand-binding site close to the membrane surface. Hydrophobic interactions and electrostatic affinity likely assist binding of the receptors with an amphiphilic ligand PA. Conductance study of the TIPS-bound receptor **1** displayed repeatable enhancement and reduction of the current-flow intensities in response to the ligand association and dissociation, respectively. Thus, reversible ligand-gated ion transportation at the bilayer is demonstrated. By spectroscopic analyses, it was suggested

that the supramolecular channels are formed upon addition of PA via multistep mechanism. Biological systems make use of various amphiphilic ligands such as epinephrine, acetylcholine, and amino acids. We believe that the present study, demonstrating the reversible ligand-gated ion transportation regulated by association/dissociation of an amphiphilic ligand, possibly leads to the development of synthetic ion channels controllable by natural as well as synthetic ligands. Such synthetic supramolecular devices would be operative in a living organism as a mimic of membrane-protein receptors and applicable for a pharmaceutical use.

EXPERIMENTAL SECTION

General Methods. ^1H , ^{13}C , and ^{31}P NMR spectra were recorded on 400 MHz FT NMR Bruker BioSpin AVANCE III 400 spectrometer or 500 MHz FT NMR Bruker BioSpin AVANCE III 500, where the chemical shifts were determined with respect to tetramethylsilane (TMS) or a residual nondeuterated solvent as an internal standard or H_3PO_4 as an external standard. Matrix-assisted laser desorption/ionization time-of-flight mass (MALDI-TOF MS) spectrometry was performed in a reflector positive mode with α -cyano-4-hydroxycinnamic acid (CHCA) as a matrix on Bruker autoflex speed, and electrospray ionization time-of-flight (ESI-TOF) MS spectra were recorded on Bruker micrOTOF-Q II-S1. UV-vis spectra were recorded on a V-530 UV-vis spectrophotometer (JASCO, Tokyo, Japan). Fluorescence spectra were recorded on an FP-6500 spectrophotometer (JASCO, Tokyo, Japan). Dynamic light scattering (DLS) was performed with a fiber-optical dynamic light-scattering spectrophotometer FDLS-3000 (Otsuka Electronics, Tokyo, Japan) and analyzed with CONTIN algorithm. Fluorescent and phase-contrast microscopy were performed with BX-51 microscope (Olympus, Tokyo, Japan), where U-MWU2 mirror unit (Excitation Filter: 330–385 nm, Emission Filter: 420 nm, Dichroic Mirror: 400 nm) was used for fluorescence observation and Olympus UPLFLN 100XO2PH (magnification: $\times 100$) was attached as the objective lens. Surface tension was measured with Kyowa Interface Science Drop Master DM 300 and analyzed by ds/de method of a pendant drop. Transmission electron micrography was conducted by Hitachi H-7650 (accelerating voltage: 80 kV).

Reagents. 2-Chloro-4*H*-1,3,2-benzodioxaphosphorin-4-one, *N,N*-dimethyl-4-aminopyridine (DMAP), 8-Hydroxypyrene-1,3,6-trisulfonic acid (HPTS), I₂, NaH, NEt(*i*-Pr)₂, (2S,SS)-2,5-hexanediol, 4-iodobenzyl bromide, Pd(PPh₃)₄, 2-phenethylamine hydrochloride (PA), and pivaloyl chloride were purchased from Tokyo Chemical Industry. 1,2-Dioleoyl-*sn*-glycero-3-phosphocholine (DOPC), 1-palmitoyl-2-stearoyl (5-doxyl)-*sn*-glycero-3-phosphocholine (5-Doxyl), 1-palmitoyl-2-stearoyl (12-doxyl)-*sn*-glycero-3-phosphocholine (12-Doxyl) and 1-palmitoyl-2-stearoyl (16-doxyl)-*sn*-glycero-3-phosphocholine (16-Doxyl) were purchased from Avanti Polar Lipids (Alabaster, AL). 1.0 M tetra-*n*-butylammonium fluoride in THF, dry triethylamine (NEt₃), and 1.0 M triethylammonium bicarbonate (TEAB, pH 8.5) buffer were purchased from Sigma-Aldrich (St. Louis, MO). Sodium thiosulfate and anhydrous Na₂SO₄ were purchased from Nacalai Tesque (Kyoto, Japan). Dry pyridine was purchased from Wako Pure Chemical Industries (Osaka, Japan). These commercial reagents were used without further purification. Anhydrous tetrahydrofuran (THF) and hexane were purchased from Kanto Chemical (Tokyo, Japan) and passed through sequential two drying columns on a Glass-Contour system just prior to use. Deionized water (filtered through a 0.22 μm membrane filter, >18.2 M Ω cm) was purified in a Milli-Q system of Millipore. Silica gel column chromatography was carried out with Silica Gel 60 (spherical, neutral, particle size: 63–210 μm) purchased from Kanto Chemical or Chromatorex-Diol silica (MB100–75/200, spherical, neutral, particle size: 110 μm) purchased from Fuji Silysia Chemical (Aichi, Japan). Thin layer chromatography (TLC) was carried out with 60 F254 purchased from Merck (Darmstadt, Germany) or Diol TLC purchased from Fuji Silysia

Chemical. Visualization of the developed chromatogram was performed by UV absorbance or I₂.

Synthesis of 3. To a dry THF (60 mL) suspension of NaH (washed twice with dry hexanes to remove mineral oil; 610 mg, 15.3 mmol) was added (2S,SS)-2,5-hexanediol (486 mg, 4.11 mmol) at 0 °C under Ar, and the resulting mixture was stirred for 1 h at 0 °C. To the reaction mixture was added 4-iodobenzyl bromide (2.56 g, 8.62 mmol), and the resulting mixture was stirred over 1.5 days at 20 °C. Then, the reaction mixture was cooled to 0 °C followed by addition of water (100 mL), and the resulting mixture was extracted with CH₂Cl₂ (100 mL, three times). The collected organic extract was washed with brine (50 mL), dried over anhydrous Na₂SO₄, and filtered off from insoluble substances. The filtrate was evaporated to dryness under reduced pressure at 30 °C, and the residue was chromatographed on silica gel (Silica Gel 60) with CHCl₃ to allow isolation of 3 (2.09 g, 3.79 mmol) as white solid in 92% yield. TLC R_f (Merck 60 F254, EtOAc/hexanes = 1/4 v/v) 0.70. ^1H NMR (500 MHz, CDCl₃ containing 0.03% TMS, 22 °C) δ 7.68 (d, J = 8.5 Hz, 4H), 7.10 (d, J = 8.0 Hz, 4H), 4.52 (d, J = 12 Hz, 2H), 4.39 (d, J = 12 Hz, 2H), 3.50 (sext, J = 5.5 Hz, 2H), 1.72–1.68 (m, 2H), 1.54–1.50 (m, 2H), 1.21 (d, J = 6.0 Hz, 6H) ppm. ^{13}C NMR (125 MHz, CDCl₃ containing 0.03% TMS, 22 °C) δ 138.85, 137.39, 129.47, 92.75, 74.89, 69.56, 32.20, 19.58 ppm. ESI-TOF MS (MeOH, positive mode) m/z calculated for C₂₀H₂₅I₂O₂ 550.9944 [M + H]⁺, C₂₀H₂₄I₂NaO₂ 572.9763 [M + Na]⁺; found 551.0181, 573.0006.

Synthesis of 4. To a dry THF (7.5 mL) and dry NEt₃ (7.5 mL) solution of 3 (610 mg, 1.11 mmol) and 2-(4-ethynylphenyl)ethanol (347 mg, 2.37 mmol) was added Pd(PPh₃)₄ (31 mg, 0.027 mmol) and CuI (20 mg, 0.11 mmol) at 0 °C under Ar. After being stirred for 13 h at 40 °C, the reaction mixture was evaporated to dryness under reduced pressure at 20 °C. To the residual yellow solid was added EtOAc (10 mL), and the resulting suspension was filtered off from insoluble substances. The orange filtrate was evaporated to dryness under reduced pressure at 30 °C, and the residue was chromatographed on silica gel (Silica Gel 60) with a gradient from CHCl₃ to CHCl₃/MeOH (20/1 v/v) to allow isolation of 4 (574 mg, 0.979 mmol) as white solid in 88% yield. TLC R_f (Merck 60 F254, CHCl₃) 0.05, (Merck 60 F254, CHCl₃/MeOH = 20/1) 0.35. ^1H NMR (400 MHz, CDCl₃ containing 0.03% TMS, 22 °C) δ 7.52 (d, J = 8.4 Hz, 4H), 7.46 (d, J = 8.4 Hz, 4H), 7.33 (d, J = 8.4 Hz, 4H), 7.22 (d, J = 8.4 Hz, 4H), 4.58 (d, J = 12 Hz, 2H), 4.46 (d, J = 12 Hz, 2H), 3.84 (t, J = 6.4 Hz, 4H), 3.52 (sext, J = 5.6 Hz, 2H), 2.87 (t, J = 6.4 Hz, 4H), 1.87 (s, 2H), 1.79–1.65 (m, 2H), 1.61–1.48 (m, 2H), 1.23 (d, J = 6.4 Hz, 6H) ppm. ^{13}C NMR (100 MHz, CDCl₃ containing 0.03% TMS, 22 °C) δ 139.3, 139.0, 131.8, 131.6, 129.1, 127.5, 122.3, 121.4, 89.2, 74.9, 69.9, 63.4, 53.5, 39.1, 32.2, 19.6 ppm. ESI-TOF MS (MeOH, positive mode) m/z calculated for C₄₀H₄₂NaO₄ 609.2981 [M + Na]⁺; found 609.3196.

Synthesis of 5. To a dry THF (5.0 mL) solution of 4 (42 mg, 0.072 mmol) and DMAP (2.0 mg, 0.016 mmol) was added dry NEt(*i*-Pr)₂ (60 μL) at 0 °C under Ar, where 4 and DMAP were dried by azeotropic dehydration from toluene at 35 °C just prior to use. Then, the resulting mixture was stirred for 5 min at 0 °C. To the resulting mixture was added 2-chloro-4*H*-1,3,2-benzodioxaphosphorin-4-one (47 mg, 0.23 mmol) promptly, and the reaction mixture was stirred for 3 h at 20 °C, where the formation of an intermediate phosphate was detected by ^{31}P NMR (CDCl₃, 23 °C, 124.33 ppm). Then, to the reaction mixture was added 1.0 M triethylammonium bicarbonate (TEAB, pH 8.5) buffer (2 mL) at 0 °C. After the resulting mixture was stirred vigorously, the supernatant organic layer was collected and dried with anhydrous Na₂SO₄. Then, the resulting mixture was filtered off from insoluble substances. The filtrate was evaporated to dryness under reduced pressure at 30 °C, and the residual yellowish oil (87 mg) was chromatographed on silica gel (Chromatorex Diol silica) with a gradient of CHCl₃/MeOH (97/3 to 95/5 v/v) to allow isolation of 5 as a NEt₃ salt (56 mg, 0.061 mmol) as colorless viscous oil in 85% yield. TLC R_f (Diol TLC, CHCl₃/MeOH = 90/10 v/v) 0.55. ^1H NMR (400 MHz, CDCl₃ containing 0.03% TMS, 23 °C) δ 7.50 (d, J = 8.4 Hz, 4H), 7.45 (d, J = 8.0 Hz, 4H), 7.32 (d, J = 8.4 Hz, 4H), 7.25 (d, J = 8.4 Hz, 4H), 4.58 (d, J = 12 Hz, 2H), 4.45 (d, J = 12 Hz, 2H), 4.12

(d, $J = 6.8$ Hz, 4H), 3.51 (m, 2H), 2.99 (m, 4H; q, $J = 7.2$ Hz, 12H, NEt₃), 1.79–1.65 (m, 2H), 1.60–1.47 (m, 2H), 1.28 (t, $J = 7.2$ Hz, 18H, NEt₃), 1.21 (d, $J = 6.0$ Hz, 6H) ppm. ¹³C NMR (100 MHz, CDCl₃ containing 0.03% TMS, 23 °C) δ 139.3, 139.3, 131.5, 131.5, 129.2, 127.5, 122.4, 121.0, 89.2, 89.0, 74.9, 69.9, 63.9, 45.3, 37.3, 32.2, 19.6, 8.5 ppm. ³¹P NMR (162 MHz, CDCl₃ containing 0.03% TMS, 6% H₃PO₄ in D₂O as an external standard in a glass capillary, 23 °C) δ 4.46 ppm. ESI-TOF MS (MeOH, positive mode) m/z calculated for C₄₆H₆₀NO₈P₂ 816.3794 [M + NEt₃ + H]⁺, C₅₂H₇₅N₂O₈P₂ 917.4999 [M + 2NEt₃ + H]⁺; found 816.3825 and 917.5030.

Synthesis of 1. To a dry pyridine (1.5 mL) solution of **5** (47 mg, 0.051 mmol) and octaethylene glycol monotriisopropylsilyl ether (88 mg, 0.17 mmol), both of which were dried by azeotropic dehydration from toluene at 35 °C just prior to use, was added pivaloyl chloride (30 μL, 0.18 mmol) at 0 °C under Ar. After the reaction mixture was stirred for 10 min at 0 °C, to the yellowish resulting suspension with white precipitates was added a mixture of I₂ (110 mg, 0.43 mmol), water (0.4 mL), and pyridine (3.0 mL) dropwise to afford red suspension. After the resulting mixture was stirred for 40 min at 20 °C, to the reaction mixture was added sat. sodium thiosulfate aq. (1 mL) at 0 °C, and the resulting mixture turned into colorless. To the resulting mixture were added TEAB buffer (pH 8.5), brine (3.0 mL), and THF (3 mL), and the resulting mixture was stirred vigorously. Then, the supernatant organic layer was collected, and dried with anhydrous Na₂SO₄. The resulting mixture was filtered off from insoluble substances, and the filtrate was evaporated to dryness under reduced pressure at 40 °C. The residual white solid (403 mg) was chromatographed on silica gel (Chromatorex-Diol silica) with a gradient from CHCl₃ to CHCl₃/MeOH (95/5 v/v) to allow isolation of **1** as a NEt₃ salt (43 mg, 0.022 mmol) as colorless viscous oil in 43% yield. TLC R_f (Diol TLC, CHCl₃/MeOH = 90/10 v/v) 0.60. ¹H NMR (400 MHz, CDCl₃ containing 0.03% TMS, 23 °C) δ 7.49 (d, $J = 8.0$ Hz, 4H), 7.43 (d, $J = 8.4$ Hz, 4H), 7.31 (d, $J = 8.4$ Hz, 4H), 7.25 (d, $J = 8.0$ Hz, 4H), 4.57 (d, $J = 12.4$ Hz, 2H), 4.45 (d, $J = 12.4$ Hz, 2H), 4.13 (sext, $J = 6.8$ Hz, 4H), 3.97 (q, $J = 6.0$ Hz, 4H), 3.94 (t, $J = 5.6$ Hz, 4H), 3.64–3.62 (m, 46H), 3.59 (t, 4H), 3.53–3.50 (m, 2H), 3.05 (q, $J = 7.2$ Hz, 12H, NEt₃), 2.97 (t, $J = 5.6$ Hz, 4H), 1.75–1.65 (m, 2H), 1.60–1.46 (m, 2H), 1.30 (t, $J = 7.2$ Hz, 18H, NEt₃), 1.21 (d, $J = 6.0$ Hz, 6H), 1.07 (m, 42H) ppm. ¹³C NMR (100 MHz, CDCl₃ containing 0.03% TMS, 23 °C) δ 139.3, 131.5, 131.44, 129.2, 127.5, 122.3, 74.9, 72.7, 70.8–70.5, 62.9, 45.7, 32.3, 19.6, 17.8, 11.9, 8.6 ppm. ³¹P NMR (162 MHz, CDCl₃ containing 0.03% TMS, 6% H₃PO₄ in D₂O as an external standard in a glass capillary, 23 °C) δ 0.10 ppm. MALDI-TOF MS (CHCA, reflector, positive mode) m/z calculated for C₉₀H₁₄₈O₂₆P₂Si₂Na [M + Na]⁺ 1785.917; found 1785.742. ESI-TOF MS (MeOH, positive mode) m/z calculated for C₉₀H₁₄₈O₂₆P₂Si₂ 1785.9170 [M + Na]⁺, C₁₀₂H₁₇₈N₂NaO₂₆P₂Si₂ 1988.1579 [M + 2NEt₃ + Na]⁺; found 1785.8696, 1988.9640.

Synthesis of 2. To a dry THF (8.0 mL) solution of **1** (80 mg, 0.041 mmol) was added 1.0 M tetra-*n*-butylammonium fluoride in THF (0.1 mL) at 0 °C under Ar. After the resulting mixture was stirred for 2 h at 0 °C, to the reaction mixture was added 1.0 M TEAB buffer (2 mL) at 0 °C. After being stirred vigorously, the supernatant organic layer was collected and dried over anhydrous Na₂SO₄. Then, the resulting mixture was filtered off from insoluble substances. The filtrate was evaporated to dryness under reduced pressure at 30 °C, and the residual colorless oil was chromatographed on silica gel (Chromatorex Diol silica) with CHCl₃/MeOH/NEt₃ (95/4/1 v/v/v) to allow isolation of **2** as a NEt₃ salt (59 mg, 0.040 mmol) as colorless viscous oil in 98% yield. TLC R_f (Diol TLC, CHCl₃/MeOH = 95/5 v/v) 0.51. ¹H NMR (400 MHz, CDCl₃ containing 0.03% TMS, 23 °C) δ 7.50 (d, $J = 8.0$ Hz, 4H), 7.44 (d, $J = 8.4$ Hz, 4H), 7.31 (d, $J = 8.4$ Hz, 4H), 7.26 (d, $J = 8.0$ Hz, 4H), 4.57 (d, $J = 12.4$ Hz, 2H), 4.45 (d, $J = 12.4$ Hz, 2H), 4.14 (sext, $J = 6.8$ Hz, 4H), 3.98 (q, $J = 6.0$ Hz), 3.95 (t, $J = 5.6$ Hz, 4H), 3.64–3.62 (m, 46H), 3.59 (t, 4H), 3.53–3.50 (m, 2H), 3.10 (br, 2H) 3.06 (q, $J = 7.2$ Hz, 12H, NEt₃), 2.97 (t, $J = 5.6$ Hz, 4H), 1.75–1.65 (m, 2H), 1.60–1.46 (m, 2H), 1.30 (t, $J = 7.2$ Hz, 18H, NEt₃), 1.21 (d, $J = 6.0$ Hz, 6H) ppm. ¹³C NMR (100 MHz, CDCl₃ containing 0.03% TMS, 23 °C) δ 139.5, 131.7, 131.46, 129.3, 127.6, 122.3, 74.9, 72.8, 70.9–70.4, 62.9, 45.8, 32.3, 11.9, 8.7 ppm. ³¹P NMR

(162 MHz, CDCl₃ containing 0.03% TMS, 6% H₃PO₄ in D₂O as an external standard in a glass capillary, 23 °C) δ 0.11 ppm. MALDI-TOF MS (CHCA, reflector, positive mode) m/z calculated for C₇₂H₁₀₆NaO₂₆P₂ [M + Na]⁺ 1471.636; found 1471.594.

Giant Unilamellar Vesicles Preparation. A typical procedure is as follows: A CHCl₃/MeOH (2/1 v/v) solution of DOPC (2.0 mM, 18 μL) and a CHCl₃ solution of **1** or **2** (2.0 mM, 2.0 μL) were mixed in a glass test tube, and the resulting mixture was gently dried under Ar flow to produce thin lipid film. The film was subsequently dried under a vacuum over 3 h and hydrated overnight with water (200 μL) at 37 °C. The final total lipids concentration was 0.20 mM.

Large Unilamellar Vesicles Preparation. A typical procedure to prepare DOPC-LUVs containing **1** in the bilayer (DOPC-**1**-LUVs) is as follows: A CHCl₃/MeOH (2/1 v/v) solution of DOPC (2.0 mM, 180 μL) and a CHCl₃ solution of **1** (2.0 mM, 20 μL) were mixed in a glass test tube, and the resulting mixture was gently dried under Ar flow to produce thin lipid film. The film was subsequently dried under a vacuum over 3 h and hydrated with water (2.0 mL) followed by freezing and thawing (five times) and 30 min sonication. Sonication was carried out under Ar at 0–5 °C using an ultrasound bath (USK-4R, 160 W).

A typical procedure to prepare DOPC-**1**-LUVs encapsulating HPTS inside the vesicles (DOPC-**1**-LUVs \supset HPTS) is as follows: A CHCl₃ solution of DOPC (2.0 mM, 180 μL) and a CHCl₃ solution of **1** (2.0 mM, 20 μL) were mixed in a glass test tube, and the resulting mixture was gently dried under Ar flow to produce a thin lipid film. The film was subsequently dried under a vacuum over 3 h and hydrated with 20 mM HEPES buffer containing 50 mM KCl (pH 7.1, 2.0 mL), 30 μM HPTS and 20 mM PA followed by freezing and thawing (five times) and 30 min sonication. The sonication was carried out under Ar at 0–5 °C using an ultrasound bath (USK-4R, 160 W). The obtained suspension was dialyzed at 4 °C in 20 mM HEPES buffer containing 50 mM KCl (pH 7.1, 1.0 L, twice) using Spectra/Por Dialysis Membrane (MWCO 3500, Spectrum Laboratories, Los Angeles, CA).

Fluorescence Depth Quenching. A CHCl₃/MeOH (2/1 v/v) solution of phosphocholines ([total phosphocholines] = 2.0 mM, 180 μL) and a CHCl₃ solution of **1** or **2** ([**1**] = [2] = 2.0 mM, 20 μL) were mixed in a glass test tube, and the resulting mixture was gently dried under Ar flow to produce a thin lipid film. The film was subsequently dried under a vacuum over 3 h and hydrated with water (2.0 mL) followed by freezing and thawing (five times) and 30 min sonication. Sonication was carried out under Ar at 0–5 °C using an ultrasound bath (USK-4R, 160 W). The phosphocholines used as the membrane constituents were DOPC alone, a mixture of 90-mol % DOPC and 10-mol % 5-, 12- or 16-Doxyl PC. To study the effect of guest binding, PA was added to the vesicle suspension in water ([PA] = 20 mM).

Binding Assay by Surface Plasmon Resonance. The interaction between PA and **1** embedded in DOPC bilayer was analyzed by surface plasmon resonance (SPR) with Biacore T200 (GE Healthcare, Buckinghamshire, UK). DOPC-**1**-LUVs ([DOPC] + [**1**] = 10 mM, [**1**]/[DOPC] = 1/9) and DOPC-LUVs ([DOPC] = 10 mM) as a reference were prepared in HEPES buffer (20 mM HEPES, 50 mM KCl, 2.0 mM MgCl₂, pH 7.5) by evaporation of CHCl₃ solution of the lipids in a glass flask, followed by vacuuming over 2 h and addition of the HEPES buffer. After vortex agitation and freezing and thawing, the resulting mixture was extruded through 50 nm membrane filter by LiposoFast Basic (Avestin, Ottawa, Canada). The LUVs suspensions were diluted to [lipids] = 0.20 mM by adding the HEPES buffer just prior to the immobilization onto the surface of a Sensor Chip L1 (GE Healthcare, Buckinghamshire, UK). The whole flow path in the instrument was washed on the basis of the manual (Desorb once, Sanitize once, and Prime three times). As a prior treatment, the sensor chip was treated with 40 mM *n*-octylglucoside (OG), which was then treated with 0.20 mM LUVs for immobilization onto the surface of the sensor chip, followed by the treatment with 50 mM NaOH for homogenization of the immobilized membrane. The sufficient immobilization of the lipids onto the surface of the sensor chip was confirmed by the adsorption amount of bovine serum albumin (BSA, 100 mg L⁻¹) to be smaller than 100 RU. All the processes were performed at 25 °C. The sensorgram was corrected for unspecific

binding and bulk refractive index effects by subtracting the signal from a reference flow cell. BIAevaluation software (GE Healthcare, Buckinghamshire, UK) was used for the analysis, where the kinetic parameters were calculated by a global fitting analysis with the assumption of the 1:1 Langmuir binding model. Dissociation constant K_d was determined from the ratio of the resultant kinetic parameters,

$$K_d = \frac{k_{\text{off}}}{k_{\text{on}}}$$

where k_{on} and k_{off} are the association and dissociation rate constants, respectively, calculated from the sensorgram.

Conductance Measurement. Ion channel current recordings of **1** and **2** were conducted as follows: Planar lipid bilayer was prepared by the reported procedure.³⁸ A mixture of DOPC (12.7 mM) and **1** or **2** (10 nM) in *n*-decane was painted on an orifice ($d = 150 \mu\text{m}$), which was sandwiched by two chambers containing HEPES buffer (upper chamber: *trans*, lower chamber: *cis*, 20 mM HEPES, 50 mM KCl, 2.0 mM MgCl₂, pH 7.5, 0.30 mL each). Current was measured with a CEZ2400 amplifier (Nihon Kohden, Tokyo, Japan) and stored on a computer using a Power Lab (AD instruments, Nagoya, Japan) at 40 kHz sampling rate. Recordings were filtered at 1 kHz. To monitor the channel current, membrane voltage was applied at 80 mV. All the current recordings were performed at 20 °C.

Fluorescence Measurement for Ion Transportation Study. To a DOPC-**1**-LUVs \supset HPTS suspension ([DOPC] = 0.18 mM, [b1] = 0.020 mM, [HPTS] = 30 μM) in 20 mM HEPES buffer containing 50 mM KCl (1.99 mL, pH 7.1) was added an aqueous solution of KOH (0.6 M, 10 μL, ΔpH = 0.8) by a syringe in the dark at 20 °C. Fluorescence intensity of HPTS at 510 nm upon excitation with 460 nm-light was monitored as a function of time until the addition of 1.0 wt % Triton X-100 (40 μL) at 100 s. Relative fluorescence intensity of HPTS entrapped in DOPC-**1**-LUVs in response to the pH enhancement was evaluated by the equation of

$$I = \frac{I_t - I_0}{I_{\text{lyzed}} - I_0}$$

where I_0 , I_t and I_{lyzed} represent the fluorescence intensities before addition of KOH, at t seconds after addition of KOH, and after lysis by the addition of 1.0 wt % Triton X-100, respectively.

Langmuir–Blodgett Monolayer Analysis. The surface pressure–area isotherm measurements and the Langmuir–Blodgett films deposition were performed with an automated Langmuir trough with a Wilhelmy type film balance HBM-AP (Kyowa Interface Science, Saitama, Japan). A CHCl₃ solution of **1**, **2**, DOPC-**1** mixture, or DOPC-**2** mixture ([b1] = [b2] = [DOPC] + [b1] = [DOPC] + [b2] = 1.0 mM, [b1]/[DOPC] = [b2]/[DOPC] = 1/9) was gently spread onto the surface of water. After still standing over 30 min at 20 °C to allow evaporation of CHCl₃, surface pressure change was monitored by moving a Teflon-coated barrier with a rate of 10 mm min⁻¹ at a constant temperature to be 20 °C.

Hydrodynamic Diameter Analysis by DOSY and Stokes–Einstein Equation. From the diffusion constant D measured by DOSY, hydrodynamic radius R_h was calculated by Stokes–Einstein equation:

$$D = \frac{k_B T}{6\pi\eta R_h}$$

where k_B , T and η represent Boltzmann constant, absolute temperature and viscosity, respectively. Reported viscosity values of the mixture of THF and water were used for the analysis.³⁹

ASSOCIATED CONTENT

Supporting Information

Absorption and CD spectroscopic studies, critical aggregation concentration evaluation, TEM, DLS, fluorescence depth quenching analyses, molecular modeling and conductance

measurements of **1** and **2**. This material is available free of charge via the Internet at <http://pubs.acs.org>.

AUTHOR INFORMATION

Corresponding Author

kinbara@tagen.tohoku.ac.jp

Notes

The authors declare no competing financial interest.

ACKNOWLEDGMENTS

We thank Prof. M. Shimomura, Prof. H. Yabu and Ms. M. Suzuki in Tohoku University for DLS measurements and transmission electron microscopic observations. We thank Prof. M. Mitsuishi and Dr. S. Yamamoto for LB monolayer analyses. We also thank Mr. K. Ichimura for assistance in analyses. This work was partially supported by Takayanagi Memorial Foundation (to T.M.), and the Ministry of Education, Culture, Sports, Science and Technology of Japan (MEXT), Grant-in-Aids for Young Scientists S and Scientific Research on Innovative Areas “Spying minority in biological phenomena (No.3306)” (23115003 to K.K.) and the Management Expenses Grants for National Universities Corporations from MEXT.

REFERENCES

- (a) Venkatakrishnan, A. J.; Deupi, X.; Lebon, G.; Tate, C. G.; Schertler, G. F.; Babu, M. M. *Nature* **2013**, *494*, 185–194. (b) Alberts, B.; Johnson, A.; Lewis, J.; Raff, M.; Roberts, K.; Walter, P. *Molecular Biology of the Cell*, 5th ed; Garland Science: New York, 2007.
- (a) Yau, K.-W. *Proc. Natl. Acad. Sci. U. S. A.* **1994**, *91*, 3481–3483. (b) Kaupp, U. B.; Seifert, R. *Physiol. Rev.* **2002**, *82*, 769–824. (c) Cascio, M. *J. Biol. Chem.* **2004**, *279*, 19383–19386. (d) daCosta, C. J. B.; Baenziger, J. E. *Structure* **2013**, *21*, 1271–1283.
- (a) Fung, B. K.-K.; Stryer, L. *Proc. Natl. Acad. Sci. U. S. A.* **1980**, *77*, 2500–2504. (b) Palczewski, K.; Kumakawa, T.; Hori, T.; Behnke, C. A.; Motoshima, H.; Fox, B. A.; Trong, I. L.; Teller, D. C.; Okada, T.; Stenkamp, R. E.; Yamamoto, M.; Miyano, M. *Science* **2000**, *289*, 739–745.
- (a) Chang, G.; Spencer, R. H.; Lee, A. T.; Barclay, M. T.; Rees, D. C. *Science* **1998**, *282*, 2220–2226. (b) *Mechanosensitive Ion Channels*; Kamkin, A., Kiseleva, I., Eds.; Springer: New York, 2008.
- (a) Osman, P.; Martin, S.; Milojevic, D.; Tansey, C. *Langmuir* **1998**, *14*, 4238–4242. (b) Kobuke, T.; Ohgoshi, A. *Colloids Surf, A* **2000**, *169*, 187–197. (c) Koçer, A.; Walko, M.; Meijberg, W.; Feringa, B. L. *Science* **2005**, *309*, 755–758. (d) Banghart, M. R.; Volgraf, M.; Trauner, D. *Biochemistry* **2006**, *45*, 15129–15141. (e) Bose, M.; Groff, D.; Xie, J.; Brustad, E.; Schultz, P. G. *J. Am. Chem. Soc.* **2006**, *128*, 388–389. (f) Jog, P. V.; Gin, M. S. *Org. Lett.* **2008**, *10*, 3693–3696. (g) Banghart, M. R.; Mourot, A.; Fortin, D. L.; Yao, J. Z.; Kramer, R. H.; Trauner, D. *Angew. Chem., Int. Ed.* **2009**, *48*, 9097–9101. (h) Liu, T.; Bao, C.; Wang, H.; Lin, Y.; Jia, H.; Zhu, L. *Chem. Commun.* **2013**, *49*, 10311–10313.
- (a) A semi-synthetic alamethicin/leucine zipper channel is reported to show reversible gating of ion transportation by iron(III). See: Kiwada, T.; Sonomura, K.; Sugiura, Y.; Asami, K.; Futaki, S. *J. Am. Chem. Soc.* **2006**, *128*, 6010–6011.
- (a) Gorteau, V.; Perret, F.; Bollot, G.; Mareda, J.; Lazar, A. N.; Coleman, A. W.; Tran, D.-H.; Sakai, N.; Matile, S. *J. Am. Chem. Soc.* **2004**, *126*, 13592–13593. (b) Talukdar, P.; Bollot, G.; Mareda, J.; Sakai, N.; Matile, S. *Chem.—Eur. J.* **2005**, *11*, 6525–6532.
- (a) Fuhrhop, J.-H.; Liman, U.; Koesling, V. *J. Am. Chem. Soc.* **1988**, *110*, 6840–6845. (b) Scrimin, P.; Tecilla, P. *Curr. Opin. Chem. Biol.* **1999**, *3*, 730–735. (c) Gokel, G. W.; Mukhopadhyay, A. *Chem. Soc. Rev.* **2001**, *30*, 274–286. (d) Bayley, H.; Cremer, P. S. *Nature* **2001**, *413*, 226–230. (e) Terrettaz, S.; Ulrich, W.-P.; Guerrini, R.; Verdini, A.; Vogel, H. *Angew. Chem., Int. Ed.* **2001**, *40*, 1740–1743.

- (f) Deamer, D. W.; Branton, D. *Acc. Chem. Res.* **2002**, *35*, 817–825.
 (g) Matile, S.; Som, A.; Sordé, N. *Tetrahedron* **2004**, *60*, 6405–6435.
 (h) Litvinchuk, S.; Bollot, G.; Mareda, J.; Som, A.; Ronan, D.; Shar, M. R.; Perrottet, P.; Sakai, N.; Matile, S. *J. Am. Chem. Soc.* **2004**, *126*, 10067–10075.
- (9) (a) Wilson, C. P.; Webb, S. *J. Chem. Commun.* **2008**, 4007–4009.
 (b) Wilson, C. P.; Boglio, C.; Ma, L.; Cockcroft, S. L.; Webb, S. *J. Chem.—Eur. J.* **2011**, *17*, 3465–3473.
- (10) (a) Muraoka, T.; Shima, T.; Hamada, T.; Morita, M.; Takagi, M.; Kinbara, K. *Chem. Commun.* **2011**, *47*, 194–196. (b) Muraoka, T.; Shima, T.; Hamada, T.; Morita, M.; Takagi, M.; Tabata, K. V.; Noji, H.; Kinbara, K. *J. Am. Chem. Soc.* **2012**, *134*, 19788–19794. (c) Shima, T.; Muraoka, T.; Hoshino, N.; Akutagawa, T.; Kobayashi, Y.; Kinbara, K. *Angew. Chem., Int. Ed.* **2014**, *53*, 7173–7178. (d) Shima, T.; Muraoka, T.; Hamada, T.; Morita, M.; Takagi, M.; Fukuoka, H.; Inoue, Y.; Sagawa, T.; Ishijima, A.; Omata, Y.; Yamashita, T.; Kinbara, K. *Langmuir* **2014**, *30*, 7289–7295.
- (11) Waybright, S. M.; Singleton, C. P.; Wachter, K.; Murphy, C. J.; Bunz, U. H. F. *J. Am. Chem. Soc.* **2001**, *123*, 1828–1833.
- (12) Marugg, J. E.; Tromp, M.; Kuyl-Yeheskiel, E.; van der Marel, G. A.; van Boom, J. H. *Tetrahedron Lett.* **1986**, *27*, 2661–2664.
- (13) DLS of **1** (5.0 mM) in THF and 1:1 mixture of THF/water displayed the particles with D_h _{THF} = 1.51 nm, D_h _{THF/Water} = 1.86 nm, respectively.
- (14) The size was calculated from the volume (1.436×10^3 nm³) computed by Molecular Mechanics with an MMFF force field using Spartan'10.
- (15) Critical aggregation concentrations (CACs) of **1** and **2** were evaluated by surface tension measurements to be ca. 0.16 and 0.20 mM, respectively. Transmission electron micrography visualized the formation of multilayer vesicles of **1** and **2** above their CACs. See Supporting Information, Figures S3 and S4.
- (16) *Circular Dichroism: Principles and Applications*, 2nd ed.; Berova, N., Nakanishi, K., Woody, R. W., Eds.; Wiley-VCH: New York, 2000.
- (17) Letsinger, R. L.; Wu, T.; Yang, J.-S.; Lewis, F. D. *Photochem. Photobiol. Sci.* **2008**, *7*, 854–859.
- (18) Akashi, K.; Miyata, H.; Itoh, H.; Kinosita, K., Jr. *Biophys. J.* **1996**, *71*, 3242–3250.
- (19) (a) Ren, J.; Lew, S.; Wang, Z.; London, E. *Biochemistry* **1997**, *36*, 10213–10220. (b) Ladokhin, A. S. *Methods Enzymol.* **1997**, *278*, 462–473. (c) Weiss, L. A.; Sakai, N.; Ghebremariam, B.; Ni, C.; Matile, S. *J. Am. Chem. Soc.* **1997**, *119*, 12142–12149.
- (20) (a) Brunsved, L.; Prince, R. B.; Meijer, E. W.; Moore, J. S. *Org. Lett.* **2000**, *2*, 1525–1528. (b) Hirschberg, J. H. K. K.; Brunsved, L.; Ramzi, A.; Vekemans, J. A. J. M.; Sibesma, R. P.; Meijer, E. W. *Nature* **2000**, *407*, 167–170. (c) van Hameren, R.; van Buul, A. M.; Castricano, M. A.; Villari, V.; Micali, N.; Schön, P.; Speller, S.; Scolaro, L. M.; Rowan, A. E.; Elemans, J. A. A. W.; Nolte, R. J. M. *Nano Lett.* **2008**, *8*, 253–259.
- (21) Addition of water into a THF solution of **1** shows blue-shift of the absorption bands and red-shift of the fluorescence bands ([**1**] = 3.4 μ M; $\lambda_{\text{Abs}}(\epsilon)$ = 288 (7.9×10^4) and 307 (6.1×10^4) nm, $\lambda_{\text{Flu}} = 340$ nm in THF; $\lambda_{\text{Abs}}(\epsilon)$ = 286 (7.4×10^4) and 304 (5.9×10^4) nm, $\lambda_{\text{Flu}} = 382$ nm in water). Likewise, addition of *n*-hexane into a THF solution of **1** shows similar spectral changes ([**1**] = 3.4 μ M, $\lambda_{\text{Abs}}(\epsilon)$ = 286 (7.4×10^4) and 305 (5.5×10^4) nm, $\lambda_{\text{Flu}} = 375$ nm in THF/*n*-hexane = 80/20), suggesting the tendency of the DPA units of **1** to be stacked in a paraffinic medium.
- (22) Isotherms of Langmuir–Blodgett monolayers composed of **1** and **2** showed a large difference in the areas per molecule, $A_1 = 0.96$ nm² and $A_2 = 0.43$ nm². See Supporting Information, Figure S11.
- (23) Pan, J.; Tristram-Nagle, S.; Nagle, J. F. *Biophys. J.* **2008**, *94*, 117–124.
- (24) (a) Schrader, T. *Angew. Chem., Int. Ed. Engl.* **1996**, *35*, 2649–2651. (b) Schrader, T. *J. Org. Chem.* **1998**, *63*, 264–272. (c) Herm, M.; Molt, O.; Schrader, T. *Chem.—Eur. J.* **2002**, *8*, 1486–1499.
- (25) The guest binding capabilities of **1** and **2** in aqueous media is described in the Supporting Information, Figures S15–S18.
- (26) (a) Mason, S. F.; Seal, R. H. *Tetrahedron* **1974**, *30*, 1671–1682. (b) Harada, N.; Chen, S. L.; Nakanishi, K. *J. Am. Chem. Soc.* **1975**, *97*, 5345–5352.
- (27) (a) Brocklehurst, B.; Bull, D. C.; Evans, M.; Scott, P. M.; Stanney, G. *J. Am. Chem. Soc.* **1975**, *97*, 2977–2978. (b) Hirata, Y. *Bull. Chem. Soc. Jpn.* **1999**, *72*, 1647–1664. (c) Moszynski, J. M.; Fyles, T. M. *Org. Biomol. Chem.* **2010**, *8*, 5139–5149.
- (28) Addition of PA to the both chambers across a planar membrane composed of DOPC alone hardly caused current flow. See Supporting Information, Figure S13.
- (29) On the basis of the K_d value evaluated by SPR, 2.70 pM of the complex **1**·PA is considered to exist in each side of the bilayer under this experimental condition.
- (30) Hille, B. *Ion Channels of Excitable Membranes*, 3rd ed.; Sinauer Associates: Sunderland, MA, 2001.
- (31) Smart, O. S.; Breed, J.; Smith, G. R.; Sansom, M. S. P. *Biophys. J.* **1997**, *72*, 1109–1126.
- (32) Rekharsky, M. V.; Goldberg, R. N.; Schwarz, F. P.; Tewari, Y. B.; Ross, P. D.; Yamashoji, Y.; Inoue, Y. *J. Am. Chem. Soc.* **1995**, *117*, 8830–8840.
- (33) The total concentration of PA, $[\text{PA}]_{\text{total}} = [\text{PA}] + [1\text{-PA}] + [\text{PA}\beta\text{CD}]$, decreased to 50 nM by the increase of the solvent volume. Taking into account the K_d value between βCD and PA, it is estimated that the concentration of the complex **1**·PA in each layer decreased to 0.48 pM after the addition of βCD .
- (34) The estimated concentration of **1**·PA in each layer is recovered to 2.41 pM.
- (35) (a) Kano, K.; Fendler, J. H. *Biochim. Biophys. Acta* **1978**, *509*, 289–299. (b) Clement, N. R.; Gould, J. M. *Biochemistry* **1981**, *20*, 1534–1538.
- (36) Hill, A. V. *Biochem. J.* **1913**, *7*, 471–480.
- (37) Cortes, D. M.; Cuello, L. G.; Perozo, E. *J. Gen. Physiol.* **2001**, *117*, 165–180.
- (38) Tabata, K. V.; Sato, K.; Ide, T.; Nishizaka, T.; Nakano, A.; Noji, H. *EMBO J.* **2009**, *28*, 3279–3289.
- (39) Czerepko, K. *Pol. J. Chem.* **1991**, *65*, 1809–1823.